

DIAGNOSTICS FOR SUPERCONDUCTING r.f. CAVITIES

H. Lengeler

CERN, European Organization for Nuclear Research, Geneva, Switzerland

Summary

In the past a variety of diagnostic methods have been developed which allow to sense the "overall" behaviour of superconducting r.f. cavities. Besides these methods temperature and X-ray mapping techniques as well as visual inspection give a more detailed insight into energy loss and electron phenomena of a superconducting cavity. With these techniques regions with increased r.f.-losses or electron emitting areas can be localised. It is hoped that these techniques together with surface diagnostic methods will give a better insight in the nature and causes of weak spots and will provide means for avoiding or eliminating such regions by adequate surface treatments.

Since the beginning of work on superconducting cavities the diagnostic methods allowing an information on the "inner life" of a superconducting cavity have been constantly developed and improved. In a first stage information were mainly gained by the r.f.-signals transmitted and reflected by the cavity. It is astonishing how many information a careful analysis of the amplitude, frequency and time behaviour of r.f. signals alone can already reveal like e.g. the overall losses, their nature, field and time dependence, the coupling factors, resonant and non-resonant electron loading, higher mode excitation, nature and behaviour of field limitations and breakdowns. Even some localisation of regions with increased r.f.-losses or of breakdown regions can be obtained in cavities where different modes can be excited.

During the 1970 a variety of methods have been developed and refined allowing much more specific insight in some cavity properties and their dependence on surface treatments, field level and operating temperature. They include the measurement of temperature increases at the cavity wall and the detection of electrons, X rays and light originating from the cavity. The state of the art has been reviewed recently in an excellent survey by H. Piel¹ and I therefore will concentrate in the following mainly on the latest developments and results.

1. Detection of light

We believe that visual observation of the cavity interior during operation has not yet been exploited to its full potential and could supply information on the inner life of a cavity in a simple way. There are a few possible sources of light inside a s.c. cavity. It is known that light emission can accompany electron emission and breakdown phenomena in vacuum². This light could be used for a localisation of electron sources and an analysis of its spectrum could give additional information on the nature of the emission process and the surface impurities involved. Light can also be produced by glowing microparticles which are heated up in a r.f.-field. A visual observation of parts of the cavity walls has already been applied at Cornell³

and Karlsruhe⁴ and has allowed to localise dust particles at the cavity wall. This method could be certainly used as a routine diagnostic for many cavities^(*).

2. Observation of bubbles inside the He-bath

r.f. breakdowns can be localised by the bubbles they produce inside the He-bath surrounding the cavity. Very often regions prone to breakdowns are known and by placing a few thermometer resistors above this region and by analysing the temperature signals and their time delays the breakdown point can be localised. Recently this method has allowed the localisation of thermal breakdowns due to an r.f. joint in a 500 MHz test cavity at Karlsruhe⁵.

In multicell cavities where many resistors would be needed a direct visual observation of bubbles is useful. In this way breakdowns with a stored energy down to 0.01 Ws have already been localised⁶. For cavities with a much larger stored energy a very crude observation system can already be sufficient for bubble detection. At Karlsruhe an evacuated endoscope for low temperature applications has been developed and tested⁷. We believe that such an instrument can be an excellent and very simple tool for the routine control of breakdowns in multicell cavities.

3. Temperature measurements at the cavity wall

One of the most powerful diagnostic methods is the temperature measurement of the cavity wall. There are at least two reasons for this: most energy loss mechanism one can think of in a s.c. cavity will finally heat up parts of the cavity walls. As the temperature is measured at the cavity wall phenomena can be localised with a greater precision than by any other measurement performed outside the cryostat. Since its first application at HEPL in 1972⁸ the method has been developed and refined considerably and has been mainly used for the localisation of breakdowns. Recently a major improvement of this method has been obtained by using a subcooled

(*) We note that a visual observation of the gas discharge used in He-processing or in ion bombardment cleaning of a cavity in an extremely convenient way for controlling the discharge. Another application of an optical system would be dust detection: it is known that some kinds of dust particles can be made visible by shining UV-light on a surface. In this way it could be checked during operation if dust particles originating e.g. from the vacuum system are deposited on the cavity surface where they are suspected to produce additional r.f. losses and possibly electron emission. This method is already applied successfully at CERN for checking the cleanliness of a cavity surface after a chemical treatment.

He-bath^{9,1} (typical bath conditions: $T = 2.2$ K and $p = 1000$ mbar). Its special heat transport properties combined with the use of carbon thermometers in close thermal contact with the cavity wall allows to measure temperature increases at the cavity wall with high sensitivity and spatial resolution. For cavities with a rotational symmetry having smooth outer walls a rotating frame with carbon resistors sliding under spring tension around the cavity can be used. In this way a comparatively small number of thermometers and associated information channels can give a precise temperature map of a cavity: spatial resolution of about 2 cm and a range of temperature increase from mK to about 2 K has been obtained¹⁰. In fig. 1 the layout of a 500 MHz single cell cavity to which temperature mapping has been applied is shown. In fig. 2 three typical temperature maps obtained at three different acceleration fields for this cavity are given. Fig. 3 shows a two dimensional plot of the temperature increase seen by one of the resistors. The power loss corresponding to a given temperature increase ΔT has been obtained from a calibration measurement¹¹. In fig. 4 we give a typical distribution of the mean power loss seen by the 39 resistors along the angle φ (i.e. the latitude dependence of the r.f. losses). Plots of this kind allow a comparison with the field distributions E^2 and H^2 along the coordinate s . In fig. 5 a temperature map of the 500 MHz, 4-cell cavity recently tested at CERN is shown¹².

Temperature maps of this kind have allowed to gain a more detailed and more direct insight in r.f. losses and electron loading inside a superconducting cavity. Some phenomena for which up to now only indirect evidence was available have been made directly visible. In the following I would like to illustrate this by a few examples.

(a) r.f. losses

It has since long been demonstrated that r.f. losses cannot be distributed homogeneously throughout the cavity walls from the observation of r.f. breakdowns, from an analysis of the Q value dependence on field level and by direct temperature measurements with fixed resistors. These observations have been fully confirmed by the temperature maps¹¹. In fig. 2 the inhomogeneity of the temperature increases can be clearly seen and fig. 3 confirms that r.f. losses are sometimes produced by many distinct regions and can vary considerably over distances smaller than the spatial resolution of the scanning thermometers (~ 2 cm).

Besides the normal BCS losses there exist large regions with increased losses which are mainly concentrated in the regions where the magnetic and the electric surface fields are both large. For all surface treatments which have been applied up to now to the CERN 500 MHz test cavities (i.e. chemical polishing, rinsing with methanol or water, ion bombardment cleaning and oxipolishing) r.f. losses always reach their minimum in the region where the magnetic field is at its maximum and the electric field vanishes (this region incidently always includes weldings!). Therefore we conclude that these losses cannot be explained by metallic losses alone and dielectric losses must be assumed. This conclusion is illustrated by the power loss distributions of fig. 4. The higher these losses are the more they show a dielectric behaviour. The overall field dependence of these losses which are dominating the Q values is quadratic up to the highest surface fields obtained ($E_p \sim 10$ MV/m, $H_p \sim 150$ G). The rather

uniform losses outside the high loss regions correspond to surface resistances of the order of R_{BCS} at 4.2 K and 500 MHz.

Besides these more uniform loss regions isolated points with enhanced r.f. losses have been localised in different parts of the cavity wall. A typical example is given in fig. 3(c). Lossy points of this kind can exist right from the beginning of r.f. measurements or can be produced by electron impact and probably also by dust particles falling during operation (preferentially) on the bottom parts of the cavity. These losses can be much larger than the mean cavity losses; they do not contribute significantly to the residual resistance of the cavity.

(b) Non resonant electron loading

Very interesting results have been obtained by combining temperature maps with electron trajectory calculations. In fig. 2(c) a temperature map obtained under strong electron loading conditions is shown. The dominant features are large temperature increases extending along the whole cavity body but confined to a few definite meridians. The half width of these temperature increases corresponds to a line like heat source. Temperature distributions of this kind can be fitted by the following assumption¹¹: a point like electron source (which does not show up itself in the temperature plot) emits electrons which are accelerated by the electric r.f. field and which for the TM_{010} mode remain within the meridian plane of the source. The electron impact on the wall produces the temperature distributions shown. In order to understand the nature of the electron emitting points extensive computer calculations have been made. The trajectories are calculated for different emission phases θ with respect to the electric field $E = E_0 \sin \omega t$ and each family is characterised by an emission point s_0 and the acceleration field E_{acc} . As the nature of the emission process can be either field emission or thermionic emission we have to make the further assumptions that the emission is either described by a Fowler-Nordheim law where emission phases around $\theta = 90^\circ$ are favoured, or by a Richardson law where the emission is assumed to be independent of θ . In the case of the field emission hypothesis the trajectory family has to be characterised in addition by the field enhancement factor β . The work function of the emitting source is unknown and is assumed to be equal to the one of niobium ($\phi = 4$ eV).

The power deposited by the accelerated electrons along the meridian of the source is calculated and compared with the measured power loss derived from the temperature increase along one trajectory family. A typical fit is shown in fig. 6 and allows to locate the electron source with a precision of a few mm at the cavity wall.

We have analysed up to now 19 electron trajectories, some of them at a few different acceleration fields: in no case the assumption of thermionic emission has given a reasonable fit; we therefore conclude that field emission dominates the behaviour of the electron sources. Similar conclusions have been found for the Karlsruhe 500 MHz test cavity¹³. With one exception all electron sources are located at the region of maximum electric field, i.e. at the iris rounding of the 500 MHz cavity (fig. 1). 17 out of 19 sources were located at the bottom part of the cavity which was always measured in the vertical position. This could support the idea that dust particles or condensation products from residual gases

are involved in the emission of electrons. There is another argument for the fact that localised impurities may be at the origin of electron sources and that is their small number and the dependence of this number on the electric surface field level E_s . After a standard chemical polishing of 20 μm followed by a rinsing with dust free methanol or water the source density remains astonishingly small up to the highest field levels reached. If one assumes a region for which holds $0.9 E_p < E_s < E_p$ (E_p : peak electric field) as a possible source for electron emitters then a typical source density of ~ 1 source/10 cm^2 is found. Obviously such small source densities are hard to explain by surface defects like grain boundaries, oxide inhomogeneities, microcracks, protrusions and the like. A "rare event" statistics produced e.g. by dust particles could be a possible explanation. Typically the effect of electron sources manifests itself on the temperature maps (and by X ray emission) at a field level of $E_p = 6$ MV/m; their number rises within an additional field increase of 0.2 MV/m and reaches a constant value up to the highest field values which we were able to reach ($E_p \sim 10$ MV/m). It would be again difficult to explain this step function behaviour with high density surface defects.

Temperature plots can also be combined with the excitation of other modes in a cavity. This can give additional information on the distribution and nature of r.f. losses and electron phenomena. In fig. 7 we give an example of a temperature map corresponding to a TE_{112} mode. The dipole character of this mode is clearly seen.

The temperature maps have shown that a chemical polishing of a few μm creates a new r.f. surface without memory for any previous imperfections. However, new defects always appear after such a treatment. The unequaled precision with which heat losses, quench regions and electron sources can be localised with the field mapping technique makes possible to treat specifically such imperfections without retreating the whole surface. This method has been applied at Wuppertal¹⁴ with great success to a 3 GHz 5 cell cavity. Surface defects have been removed locally by mechanical grinding followed by a slight chemical polishing of less than 5 μm . The maximum acceleration field could be increased by a threefold application of this procedure from 1.8 to 5.5 MV/m.

The possibility for localising precisely a very small number of electron sources and lossy regions on a surface with a total area of the order of ~ 1 m^2 has lead us at CERN to the development of a small scanning electron microscope which can be introduced inside a 500 MHz cavity¹⁵. Preliminary tests have shown that in some cases electron sources and isolated lossy regions can be associated with special features of the surface. The analysis of these results is going on.

Acknowledgements

I would like to thank W. Bauer, J. Halbritter and D. Proch for information on current work going on in their laboratories and the members of the CERN group as well as H. Piel for their help in the analysis of the temperature maps and for many fruitful discussions.

References

1. H. Piel, KfK Report 3019, Karlsruhe 1980, p.85
2. See e.g. R.E. Hurley, J. Phys. D: Appl. Phys. Vol. 12, 1979, p. 2229 and 2247.
3. J. Kirchgessner, H. Padamsee, H.L. Phillips, D. Rice, R. Sundelin, M. Tigner and E. Borstel, IEEE Trans. NS-22, No. 3 (1975) 1141.
4. W. Bauer, A. Citron, G. Dammertz, M. Grundner, L. Husson, H. Lengeler, E. Rathgeber, *ibidem* p. 1144 (1975).
5. W. Bauer, private communication.
6. A. Citron, G. Dammertz, M. Grundner, L. Husson, R. Lehm and H. Lengeler; Nucl. Instr. and Methods 164 (1979) 31.
7. A. Brandelik, private communication.
8. C.M. Lyneis, M. McAshan and N.T. Viet, Proc. of 1972 Proton Lin. Acc. Conf. Los Alamos (1972) 98.
9. H. Piel and R. Romijn, CERN Internal Report, CERN/EF/RF 80-3 (1980).
10. P. Bernard, G. Cavallari, E. Chiaveri, E. Haebel, H. Heinrichs, H. Lengeler, E. Picasso, V. Picciarelli and H. Piel; Proc. 11th Int. Conf. on High Energy Acc., Geneva (1980) 878.
11. P. Bernard, G. Cavallari, E. Chiaveri, E. Haebel, H. Heinrichs, H. Lengeler, E. Picasso, V. Picciarelli, J. Tückmantel and H. Piel, to be published in Nucl. Instr. and Methods.
12. P. Bernard, G. Cavallari, E. Chiaveri, E. Haebel, H. Lengeler, J.M. Maugain, E. Picasso, V. Picciarelli, J. Tückmantel and W. Weingarten, CERN Internal Report CERN/EF/RF 81-2 (1981).
13. Sh. Noguchi, Y. Kojima and J. Halbritter, Nucl. Instr. and Meth. 179 (1981) 205.
14. T. Grundey, U. Klein and D. Proch, this conference.
15. A. Mathewson and A. Grillot, private communication.

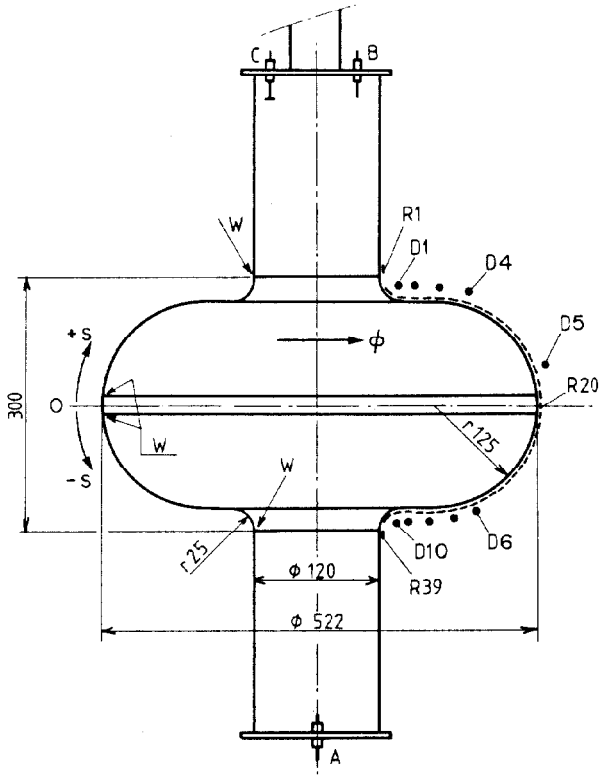


Fig. 1 Layout of 500 MHz test cavity. A: r.f.-input; B, C; r.f. probes, D1-D10: X-ray detectors, R1-R39: resistors for temperature mapping; W: weldings. The coordinate system used is indicated. Dimensions are in mm.

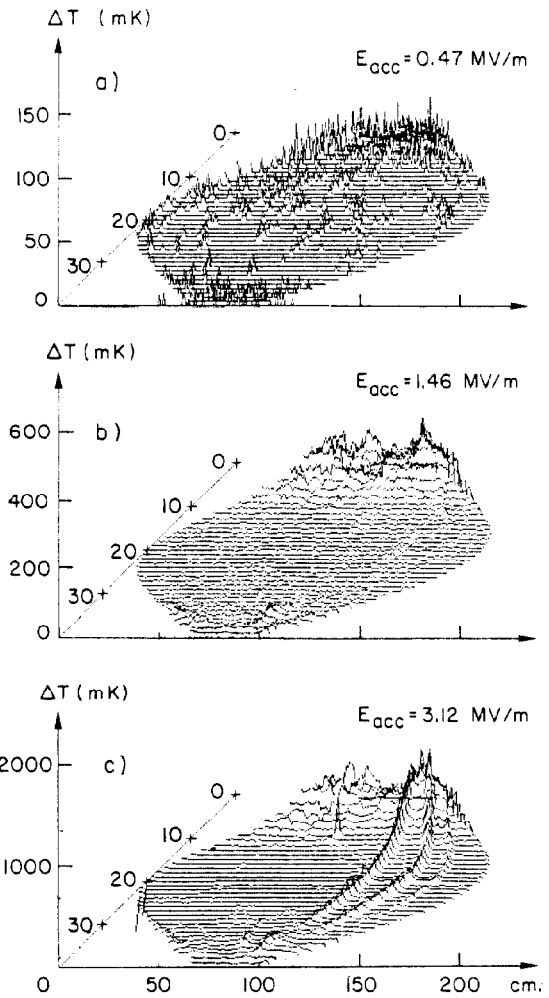


Fig. 2 Temperature map of the cavity of fig. 1 for three different accelerating fields. The surface of the cavity body is projected on a plane. On the x axis the distance along a circle of constant latitude is plotted. The y axis shows the number of resistors. The temperature increases are plotted along the z axis.

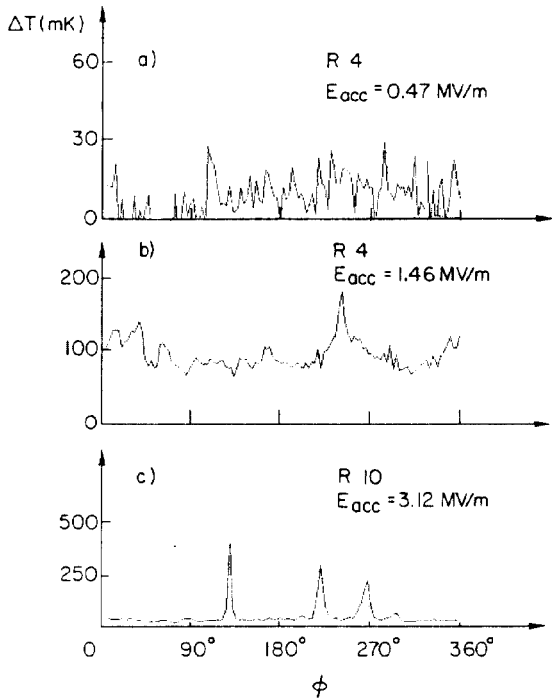


Fig. 3 (a,b) Temperature profiles measured by resistor 4 along its path around the cavity for 2 different acceleration fields. (c) Same for resistor 10. The peak at $\phi = 130^\circ$ corresponds to a lossy point, the two other peaks correspond to electron trajectories.

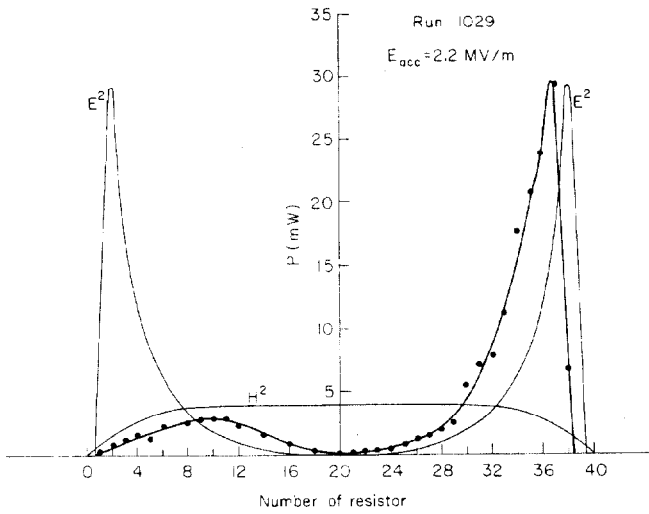


Fig. 4 Mean value of r.f. power dissipated at the cavity wall for the 39 resistors. The power losses are integrated over the angle $\varphi = 0^\circ - 360^\circ$ and show a strong up-down asymmetry. For comparison the E^2 and H^2 distribution for the $TM_{0,10}$ mode are given.

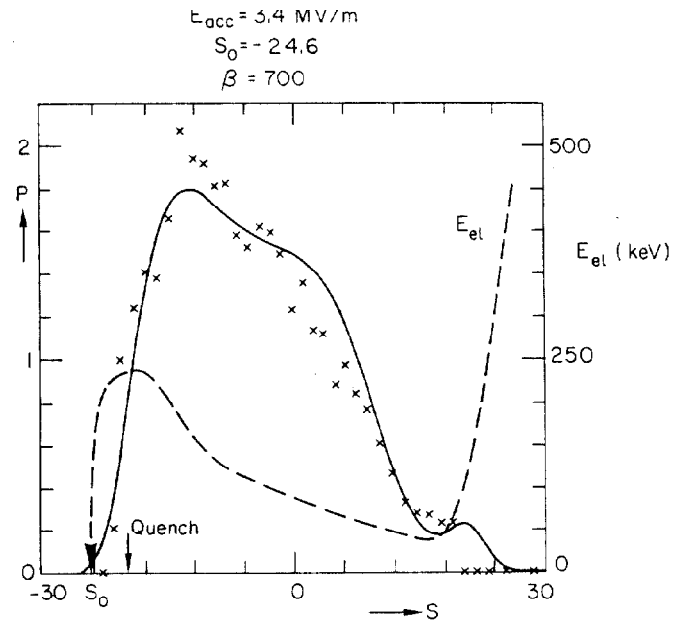


Fig. 6 Fit of measured power loss of an electron trajectory family along its meridian. The measured values are indicated by crosses. The fit parameters and the electron impact energies are also given. The source location is indicated by an arrow.

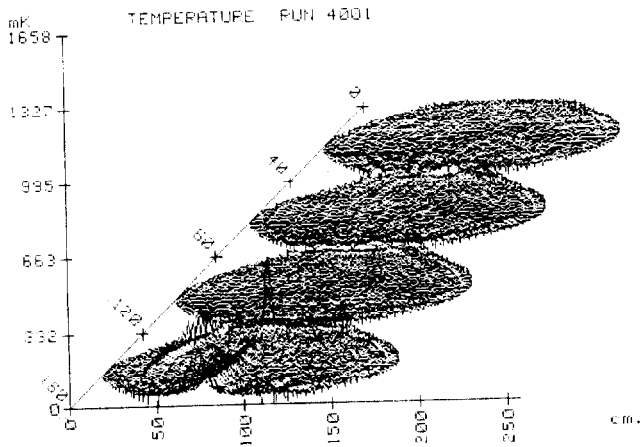


Fig. 5 Temperature map of a 4-cell 500 MHz acceleration cavity operated in a π -mode. The map is similar to the one of fig. 2. r.f.-losses are concentrated at the bottom cell. $E_{acc} = 2$ MV/m.

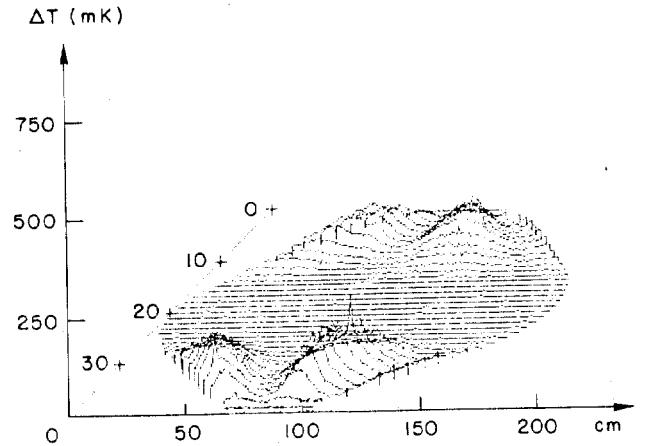


Fig. 7 Temperature map of the one-cell 500 MHz test cavity excited in a $TE_{1,12}$ -mode.